Acta Geotechnica
https://doi.org/10.1007/s11440-026-03009-2

RESEARCH PAPER

Interface characterization of ground anchors embedded in soybean urease-induced carbonate precipitation-stabilized soils

Genbao Zhang[1,2] · Xiao Luo[3] · Siqing Li[1] · Lanting Deng[3] · Yukang Liu[1] · Zhining Wang[1] · Zhongbiao Li[1] · Mingdong Li[4] · Changjie Xu[2]

Received: 8 September 2025 / Accepted: 2 March 2026

Abstract
Due to the long-term strength degradation of soils, ground anchors often exhibit insufficient anchorage performance during service. Reinforcing the soil around anchors using soybean urease-induced carbonate precipitation (SICP) technology is a potential method to enhance the anchorage performance of active anchors. To explore the mechanism of anchorage performance evolution of SICP-stabilized anchors and the impact pattern of cementation solution concentration on reinforcement effectiveness, urease activity selection tests were conducted to determine the soybean powder concentration for SICP-stabilized soil. Cementation solutions with equal mass ratios of calcium chloride and urea were prepared, and samples of and element specimens of SICP-stabilized anchors were made under different cementation solution concentrations. Direct Shear tests on stabilized soil and interface shear tests on stabilized anchors were performed. Microstructural tests, including XRD and SEM, were also conducted on the stabilized soil within the shear bands of the stabilized anchors. The study found that SICP-stabilized soil exhibits strain-hardening behavior under shear. Cohesion and internal friction angles show a "see-saw" complementary relationship with increasing cementation solution concentration. The bond-slip at the SICP-stabilized anchorage interface exhibits strain-softening behavior. Once the cementation solution concentration exceeds 1.00 mol/L, the peak shear strength of the anchorage interface increases linearly with further concentration increases. However, the residual shear stiffness of the anchorage interface is less sensitive to changes in cementation solution concentration. Microstructural analysis reveals 1.75 mol/L as a critical threshold. At this concentration, $CaCO_3$ phase transformation homogenized the pore structure and formed a strong interfacial cementation layer, which enhanced the interface shear strength, initial shear stiffness, and soil cohesion.

Keywords Cementation solution concentration · Interface characterization · Shear strength · SICP · Soil anchors

1 Introduction

In geotechnical engineering, anchor grouting technology is widely used to maintain or enhance the stability of geotechnical bodies, creating a large number of active anchor structures, including soil anchors along highways and municipal roads [10, 21]. The anchorage performance of soil anchors can degrade or even fail [20, 39, 41] during service due to the combined effects of soil creep [32, 35] and environmental factors like wet-dry cycles [23], threatening slope stability and making reinforcement of soil anchors urgently needed.

Under the "dual carbon" goals, bio-mineralization via bio-enzyme induced $CaCO_3$ deposition has matured and is now widely used in foundation treatment, geotechnical reinforcement, and environmental remediation [2, 14, 36]. The process involves urease catalyzing urea hydrolysis to produce CO_2 and NH_3. The NH_3 then triggers ammonia equilibrium reactions to raise hydroxide ion levels, creating an alkaline environment. In this setting, CO_2 and NH_3 react to form HCO_3- and CO_3^{2-}. Adding soluble calcium sources like $CaCl_2$ enables calcite reactions between Ca^{2+} and CO_3^{2-}, yielding $CaCO_3$ precipitates. Based on how urease is introduced, methods using intracellular urease from bacterial culture are called MICP (Microbially Induced Carbonate Precipitation) [17, 25, 37], while those using urease directly extracted from plants are termed EICP

Extended author information available on the last page of the article

Published online: 21 March 2026

(Enzyme Induced Carbonate Precipitation) [29–31]. EICP, not requiring bacterial culture and less oxygen-dependent, is ideal for reinforcing fine-pored clay. Among EICP plants, soybeans, due to their large scale and high yield, are the main urease source, forming SICP (Soybean urease-induced carbonate precipitation) [7, 8, 13, 15, 16, 28, 38, 40]. This SICP technology has achieved good results in desert control, fracture repair, and foundation reinforcement [11, 12, 19, 26], showing great potential for extension in soil anchor reinforcement.

Currently, there are no literature reports on SICP technology for soil anchor reinforcement. This is mainly due to two reasons. Firstly, the anchorage performance of soil anchors depends on the soil strength at the shear band of the anchorage interface. Compared to the anchor spacing, the shear band range is small, making precise bio-mineralization of the soil in this band challenging. Secondly, soil anchor slopes are existing geotechnical structures. Introducing urease and cementation solution into the soil around anchors requires special grouting equipment, posing construction challenges. Given these challenges, the application effects of SICP and other bio-mineralization technologies on soil anchors need comprehensive evaluation to ensure their technical and economic advantages for promotion.

Therefore, this paper will comprehensively evaluate the effectiveness of SICP technology in enhancing the anchorage performance of soil anchors. It will explore how cementation solution concentration affects the mechanical properties of SICP-stabilized soil and anchors. Specifically, it will determine the optimal soybean powder concentration for SICP-stabilized soil samples under maximum urease activity through urease activity experiments. It will also establish the development pattern of shear strength parameters in SICP-stabilized soil with increasing cementation solution concentration using direct shear tests. Additionally, it will investigate the evolution of the anchorage interface shear properties of SICP-stabilized anchors at different cementation solution concentrations through pullout tests. Finally, it will analyze the composition and microstructure of the soil at the shear band of the SICP-stabilized anchorage interface via SEM and XRD tests.

2 Materials and methods

2.1 Soil properties

The soil used in the experiment was obtained from the planned reserve area of Hunan City University and belongs to the lacustrine sedimentary layer of the Dongting Lake. The soil samples were obtained from a depth of 0.5–0.7 m. The representative soil was classified according to the current Chinese national standard GB/T 50145-2007 and was identified as silty sand, SM (clayed sand, SC in ASTM D2487-2017). After collecting the soil, plant roots and other debris were removed from the original soil, and it was sieved through a 5-mm sieve and then dried. In accordance with the "Standard for Geotechnical Test Methods (GB/T 50123-2019)", basic physical property tests of the soil were carried out. As the soil was sourced and all experiments were performed locally, the Chinese national standards were followed for sample preparation and testing to ensure methodological consistency and reliability. The gradation curve of the soil is shown in Fig. 1a. The various physical properties of the soil are presented in Table 1.

2.2 Urease properties

To extract urease with effective activity from soybean powder, solutions of different soybean powder concentrations were first configured in gradients. Then, the urease activity was measured to obtain the relationship curve between urease activity and soybean powder concentration. Finally, the soybean powder concentration with the highest urease extraction efficiency was selected.

2.2.1 Extraction of soybean urease solution

To obtain soybean urease solution from commercially available regular soybean powder, the following steps are performed:

(1) A concentration gradient of soybean powder solution was established (as shown in Table 2), with corresponding masses of soybean powder being weighed and dissolved in 100 mL of deionized water. After thorough mixing, the solution was allowed to stand for 3 h.
(2) Then, the supernatant was centrifuged at 4000 rpm for 15 min (20 ± 1 °C).
(3) After observing the separation of soybean residue in the centrifuge tube, the supernatant was collected and filtered through filter paper to obtain the soybean urease solution.

2.2.2 Determination of soybean urease activity

The activity of soybean urease was determined using a conductivity meter. The conductivity meter used in this study was a DDS-11A laboratory conductivity meter. Before testing, the instrument was calibrated with a standard solution of known precise conductivity (1413 μS/cm)

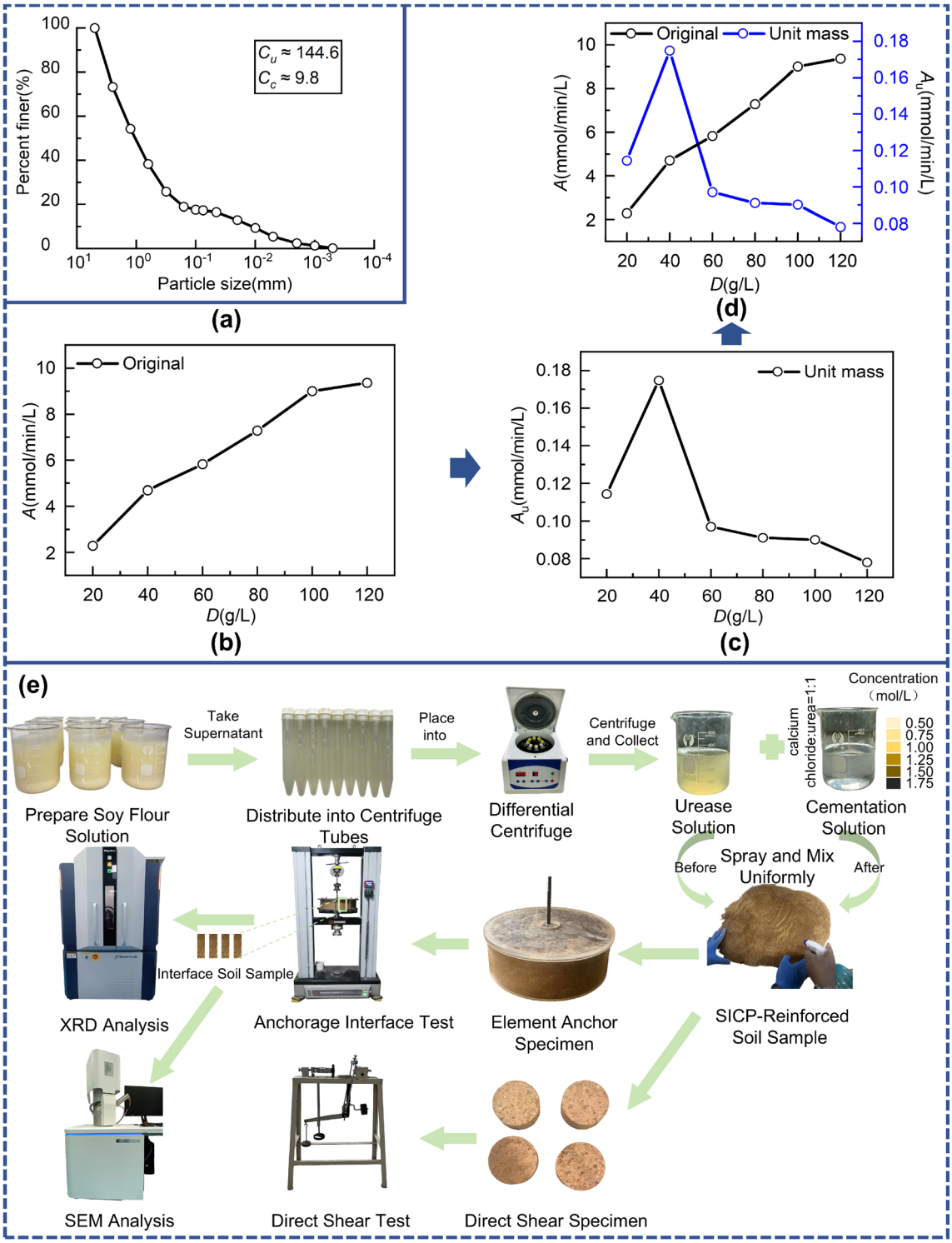

Fig. 1 **a** particle size distribution curve of the soil; variation of urease activity at different soybean powder concentrations: **b** original, **c** unit mass, **d** total, A represents urease activity, A_u represents urease activity per unit mass, and D represents soybean powder concentration; **e** the experimental flowchart in this study

Table 1 The physical and mechanical properties of the soil sample

Properties (unit)	Value
Plastic index, PI (%)	19.0
Liquid limit, LL (%)	35.2
Uniformity coefficient, C_u	144.6
Coefficient of curvature, C_c	9.8
Natural moisture content, w_{opt} (%)	24.0%
Natural density, ρ_n (g/cm^3)	1.554
Cohesion, c (kPa)	61.8
Internal friction angle, φ (°)	16.7

Table 2 Soybean powder solution concentration gradients

Test number	1	2	3	4	5	6
S/L ratio	1:50	1:25	1:16.7	1:12.5	1:10	1:8.3
Soybean powder concentration (g/L)	20	40	60	80	100	120

to ensure the accuracy of the measurement data. To assay urease activity at different soybean powder concentrations:

(1) 1.8 g of urea was weighed and dissolved in 27 mL of deionized water.
(2) 3 mL of the soybean urease solution to be tested was taken and added to the urea to prepare a mixed solution, with the initial concentration of urea being 1 mol/L after mixing.
(3) The change in conductivity of the mixed solution within 15 min was measured using a conductivity meter at room temperature 20 ± 1 °C (controlled by air conditioning), with conductivity values recorded every 5 min.

Urease activity was characterized by the amount of urea hydrolyzed per minute per liter of urease extract, expressed as mmol/(minL). A conductivity change of 1 mS/cm/min corresponds to a urea hydrolysis rate of 11.11 mmol/(minL). The urease activity can be obtained by converting the measured average change in conductivity per minute into the amount of urea hydrolyzed per minute and then multiplying by the dilution factor of 10 [22]. Additionally, the extraction efficiency of soybean urease for SICP technology was evaluated by the urease activity per unit mass of soybean powder. A higher value indicates a more efficient extraction [26]. The urease activity can be calculated using Eq. (1):

$$A = \frac{\Delta\kappa}{\Delta t} \times 11.11 \times m \quad (1)$$

where $\Delta\kappa/\Delta t$ is the slope of conductivity change over time (mS/cm/min); m is the dilution factor of the urease extract in the reaction system (which is 10 in this study); the coefficient 11.11 is an empirical conversion factor, a conductivity change of 1 mS/cm/min corresponds to a urea hydrolysis rate of 11.11 mmol/(minL).

As shown in Fig. 1b–c, the urease activity (A) varies with the soybean powder concentration. Like prior studies [9, 27], the urease activity per unit mass (A_u) of soybeans peaks at a certain concentration, reaching the maximum at 40 g/L. This indicates that the extraction efficiency is highest at this concentration. Thus, 40 g/L soybean powder was chosen for urease extraction in this experiment.

2.3 Preparation of cementation solution

Calcium chloride offers a calcium source for calcium carbonate deposition, and urea provides nitrogen for microbial growth. For the experiment, calcium chloride and urea from Macklin were mixed in a 1:1 mass ratio to form the cementation solution. Based on literature on SICP-stabilized soil, the cementation solution concentrations were set as follows: 0.00, 0.50, 0.75, 1.00, 1.25, 1.50, and 1.75 mol/L.

3 Experimental programs

To investigate how cementation solution concentration affects the mechanical properties of SICP-stabilized soil and anchors, a series of experiments were conducted. These included direct shear tests on SICP-stabilized soil at different cementation solution concentrations, interface shear tests on SICP-stabilized anchors, and microstructural analysis of the soil in the shear band of the anchorage interface. The experimental flowchart is outlined in Fig. 1e.

3.1 Specimen preparation

3.1.1 Element anchor specimens of the SICP-stabilized soil

The author's team developed anchorage interface shear testing technology based on the element concept, which has been successfully applied to various anchors [4, 5, 33]. This study used this technology for anchorage interface shear testing of SICP-stabilized soil anchors. Per the testing requirements, an element anchor sampling device was used, as shown in Fig. 2b. The size parameters of the SICP-stabilized soil element anchor specimens are: specimen diameter 300 mm, specimen height 100 mm, anchorage body height 80 mm, and anchorage body diameter 48 mm (as shown in Fig. 2a). The prepared specimens are shown

in Fig. 2c. One element anchor specimen was prepared for each cementation solution concentration group. The temperature during specimen preparation and curing was maintained at 20 ± 1 °C (controlled by air conditioning). The specific preparation steps are as follows:

(1) SICP-stabilized soil samples were prepared. The aqueous solution was replaced with a mixture of soybean urease solution and cementation solution. The spray-mixing method was used to incorporate the mixture into dry soil [3, 18, 24]. The water content of the soil sample was adjusted and controlled at 24.0% (as the mass ratio of the urease and cementation solutions to the dry soil). During mixing, a predetermined amount of dry soil was first weighed; the soybean urease solution was then sprayed in batches onto the dry soil using a spray bottle, with thorough mixing after each spraying. After the mixture had stood for 1 h, the cementation

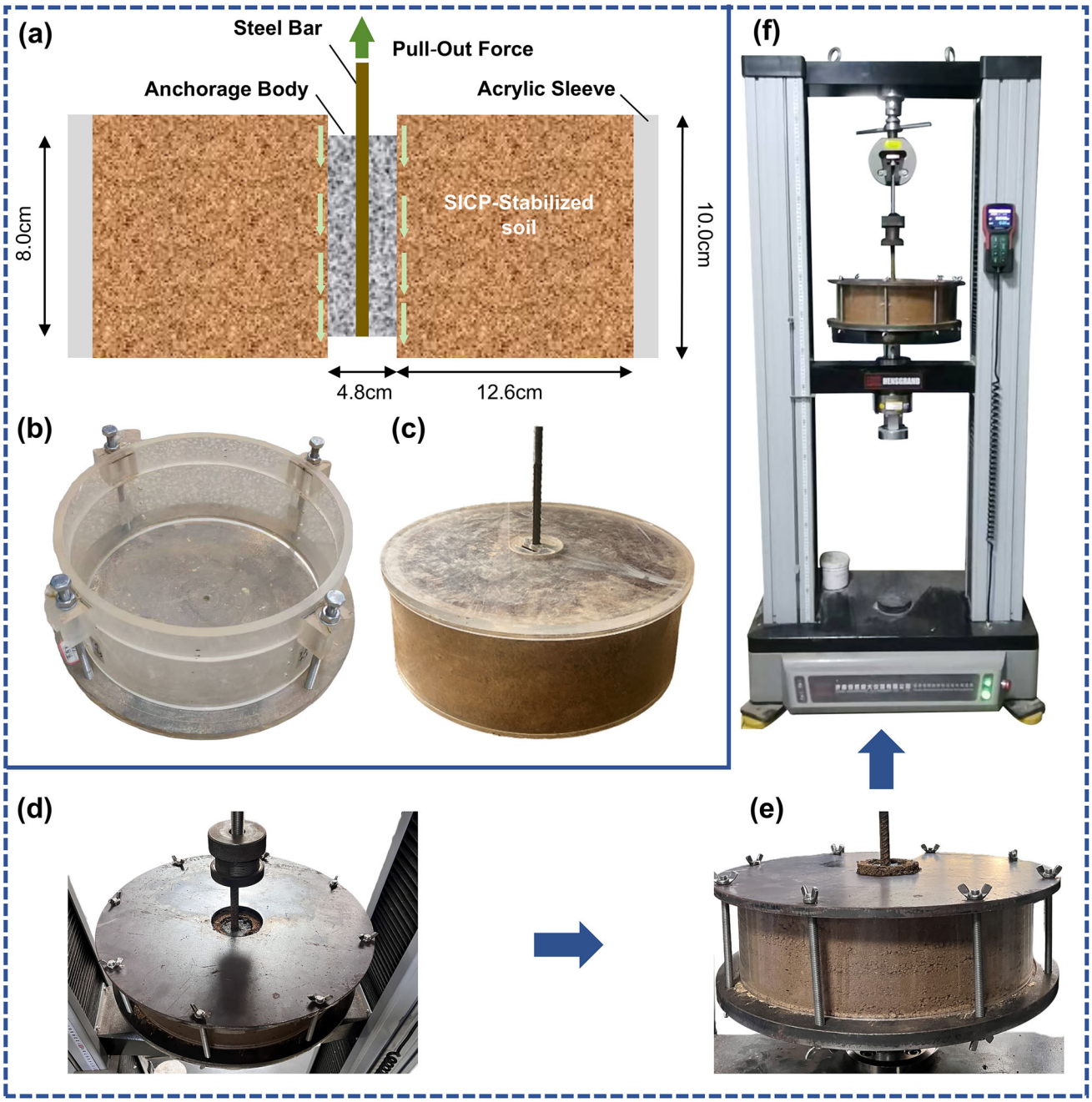

Fig. 2 Dimensions of the element specimen, the sampling device, and the finished specimen: **a** the size of the specimen, **b** the mold, **c** the specimen after preparation; the loading device and its arrangement: **d** top view, **e** front view, **f** general view

solution was sprayed onto the soil sample using the spray bottle. The soil was mixed thoroughly and then placed in a sealed bag for 24 h of curing.

(2) SICP-stabilized soil compaction: The dry density of the soil in the element anchor specimen was controlled at 1.685 g/cm^3. The total amount of soil required for each specimen was estimated based on the specimen dimensions, and after weighing, the soil was poured into the mold in five separate layers for compaction. Each layer was compacted to a thickness of approximately 2 cm. Prior to compaction, the soil samples were leveled, and geotextile was placed to prevent surface tilting of the compacted soil. After each layer was compacted, the surface of the soil was scarified with a spatula to prevent delamination between layers. Before compaction, a steel pipe reserved for the anchor hole at the center of the specimen was coated with Vaseline and wrapped with PVC film to prevent damage to the surrounding soil during subsequent pipe extraction.

(3) Pipe Pulling and hole forming: After the nut and pressure plate of the mold were removed, and the centering rod and centering device were taken out, the steel pipe was gripped and rotated inward while being wrapped in PVC film, then extracted to form the anchor hole for the element anchor specimen. Compared to the drilling method, the pre-formed hole method was used to create the anchor hole for the element specimens in this experiment, which was primarily based on considerations of experimental efficiency and operability.

(4) Grouting and curing: The acrylic base plug of the mold was installed; a steel bar was placed at the center of the anchor hole; and a centering device was placed on the upper part of the steel bar. Cement mortar was prepared with a water–cement ratio of 0.45; the anchor hole was filled with the cement mortar, which was stirred using a thin iron wire. After initial setting of the mortar, the centering device and the base plug were removed. The specimen was sealed in a bag and cured for 7 days.

It should be noted that author team's prior research revealed a key finding: under actual construction methods that simulate stress release processes, the magnitude and development of the shear strength at the anchor-soil interface are almost independent of ground pressure [6]. Therefore, to simplify the experimental procedure, an unconfined (free boundary) design scheme was adopted. When the diameter ratio between the specimen and the anchorage body exceeds 5, the influence of boundary conditions on the interface shear behavior can be eliminated [6], provided that the element anchor specimen is unconfined. In this study, the ratio is $6.25 > 5$. Thus, the effect of boundary conditions is minimal and can be neglected.

3.1.2 Direct shear specimens of the SICP-stabilized soil

In accordance with the "Standard for Geotechnical Test Methods (GB/T 50123-2019)", direct shear test specimens were prepared from SICP-stabilized soil that had been cured for 24 h. Eight direct shear test specimens were prepared for each cementation solution concentration group. After preparation, the direct shear test specimens were left to cure for an additional 7 days.

3.2 Direct shear test of the SICP-stabilized soil specimens

The direct shear test is a widely accepted and practical method for evaluating the relative improvement in bio-cemented soils [1, 3]. In this study, direct shear tests were conducted on SICP-stabilized soil specimens under different cementation solution concentrations. For each concentration, eight shear specimens (two parallels per group) were tested under four normal pressures: 100, 200, 300, and 400 kPa (as shown in Fig. 3a). The shear rate was 0.8 mm/min. The specimen height is 20 mm, and the diameter is 61.8 mm (standard size). Experimental steps followed the "Standard for Geotechnical Test Methods (GB/T 50123-2019)".

3.3 Interface shear test of the SICP-stabilized anchors

The author's team developed anchorage interface shear testing technology to conduct pullout tests on SICP-stabilized element anchor specimens, obtaining bond-slip curves. A universal testing machine (HST WDW-50D) was modified for testing, using constant-rate loading at 1 mm/min. The pullout distance of the specimen was 20 mm [4]. Pull force and displacement were monitored in real-time via a data acquisition platform. The specifications of the testing machine are listed in Table 3. The loading device and its arrangement are shown in Fig. 2d–f. For detailed steps, refer to the team's published literature [6, 34, 42].

3.4 Microstructural analysis of shear band soil at the SICP-stabilized anchorage interface

To investigate the microstructural mechanisms of how SICP reinforcement affects the shear properties of the anchorage interface under different cementation solution concentrations, soil samples were taken from the shear band near the bonding interface of the specimens after the

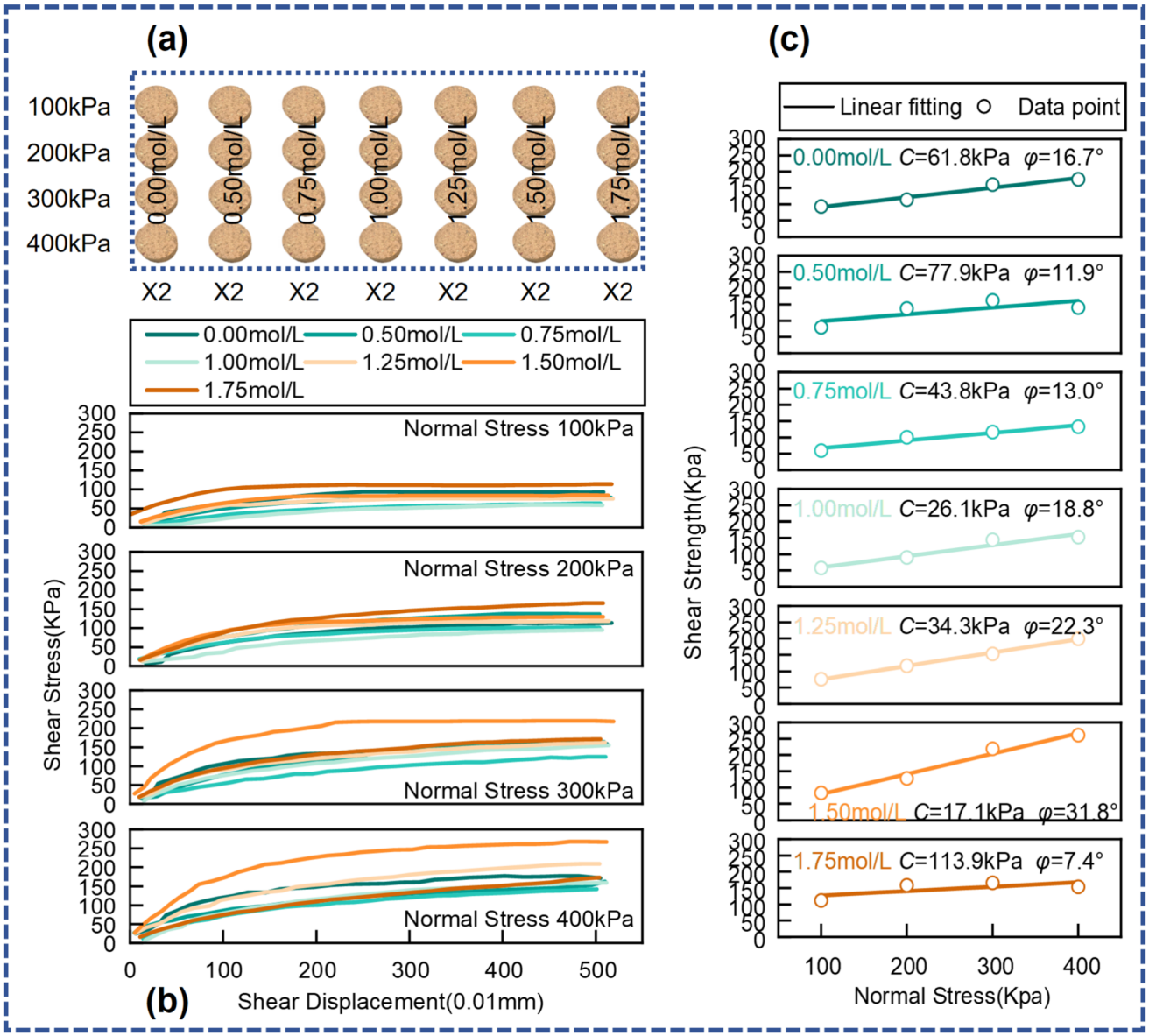

Fig. 3 **a** specimens required for direct shear tests; **b** shear stress-displacement curves of SICP-stabilized soil specimens at different cementation solution concentrations: from top to bottom, 100 kPa, 200 kPa, 300 kPa, and 400 kPa; **c** shear strength curves of SICP-stabilized soil at different cementation solution concentrations: from top to bottom, 0.00 mol/L, 0.50 mol/L, 0.75 mol/L, 1.00 mol/L, 1.25 mol/L, 1.50 mol/L, 1.75 mol/L

Table 3 The specifications of the testing machine

Parameter	Specification
Model	HST WDW-50D
Maximum load capacity	50 kN
Speed control range	0.01–1000 mm/min
Displacement resolution	0.4 μm
Force accuracy	$\leq \pm 0.5\%$

anchorage interface testing was completed. Given the significant scale difference between the macroscale shear band and the microscale features of interest (e.g., particle contacts and $CaCO_3$ crystals), representative soil samples could be obtained without compromising their microstructure. These samples were then carefully handled and prepared for SEM. SEM analysis was performed on the shear band soil samples using a Czech TESCAN MIRA LMS scanning electron microscope to obtain the structural characteristics and pore size distribution patterns of the samples. XRD analysis was conducted on the shear band soil samples using a Japanese Rigaku Smart Lab SE energy spectrometer to evaluate the mineralization effects. The X-ray diffractometer was set with a scanning range of 10–80° and a scanning speed of 2°/min.

4 Results and analysis

4.1 Shear strength properties of the SICP-stabilized soil samples

4.1.1 Parameters of shear strength

The shear stress–displacement curves obtained from the direct shear tests of SICP-stabilized soil specimens at different cementation solution concentrations are shown in Fig. 3b. The shear response of the SICP-stabilized soil specimens is characterized by strain hardening. Under the same cementation solution concentration, the normal stress has a significant effect on the hardening characteristics. At low normal stresses (e.g., 100 kPa), the degree of hardening is limited, and the soil gradually exhibits plastic flow behavior. In contrast, at higher normal stresses, the hardening characteristics become more pronounced. However, the sensitivity to normal stress decreases, leading to the convergence or even overlap of the strain-hardening curves under different normal stresses (e.g., the curves for 300 kPa and 400 kPa). It can be inferred that increasing the normal stress enhances the shear stiffness of the SICP-stabilized soil, enabling it to better resist large deformations. Nonetheless, a threshold for normal stress exists beyond which the effect of normal stress on improving shear stiffness becomes less significant.

Due to the strain-hardening behavior of SICP-stabilized soil specimens in shear, the shear stress–displacement curves show no distinct stress peaks. Following the data processing requirements for direct shear tests in the "Standard for Geotechnical Test Methods (GB/T 50123-2019)", the shear stress corresponding to a displacement of 400 mm is defined as the shear strength. The resulting shear strength curves for SICP-stabilized soil specimens are shown in Fig. 3c. The curves demonstrate a largely linear relationship under different cementation solution concentrations. However, the overall distribution exhibits noticeable clustering with varying concentrations, such as at 0.75 and 1.00 mol/L. This requires further analysis.

4.1.2 Effect of the cementation solution concentration

As shown in Fig. 4a, the shear strength parameters (cohesion and internal friction angle) of SICP-stabilized soil vary with cementation solution concentration. Cohesion initially decreases and then increases with rising concentration, forming a "valley-shaped" trend, while the internal friction angle first increases and then decreases, forming a "peak-shaped" trend. At a concentration of 1.50 mol/L, the internal friction angle peaks at 32.0°, and cohesion reaches its minimum of 17.1 kPa. Notably, the variation trends of cohesion and internal friction angle with cementation solution concentration present a "see-saw" complementary relationship (i.e., an increase in cohesion often leads to a decrease in the internal friction angle). However, between concentrations of 1.00 and 1.25 mol/L, both cohesion and the internal friction angle increase.

Further analysis of the variation trends shows that, given a specific urease activity (from the fixed soybean powder concentration in this test), the amount of urea hydrolysis catalyzed by a certain amount of urease is limited after the cementation solution (a mixture of urea and calcium chloride) is added. This leads to a fixed amount of carbonate ions from hydrolysis and a corresponding fixed amount of calcifiable calcium ions. Thus, the calcium carbonate deposition catalyzed by a specific urease amount is limited. Therefore, there must be an optimal mass ratio of urea to calcium chloride for a given urease amount. However, this optimal ratio is influenced by the soil's mineral composition, which varies among soils and creates different carbon and ammonia equilibria environments within the soil structure. This alters the degree of "mineralization reactions". Since the cementation solution used in this test is prepared with a 1:1 mass ratio of urea to calcium chloride, it does not align with this optimal ratio. Consequently, variations in cementation solution concentration fail to achieve optimal calcium carbonate mineralization, resulting in fluctuations in the shear strength parameters (c, φ) of SICP-stabilized soil.

The carbonate generated in the mineralization reaction influences soil strength through "chemical bridging" and "physical roughening". "Chemical bridging" occurs when amorphous carbonate forms stable calcite crystals between adjacent soil particles, enhancing cohesion by binding and filling the particles. In contrast, "physical roughening" happens when amorphous carbonate crystallizes on individual soil particles, breaking existing particle contacts and reducing cohesion, while increasing the surface roughness of the particles and thus the internal friction angle.

In this experiment, when the cementation solution concentration is low (below 1.00 mol/L), calcium carbonate crystals primarily undergo heterogeneous nucleation and growth at defects on the soil particle surfaces (i.e., "physical roughening"). This growth directly increases the surface roughness of the particles, which is the main reason for the increase in the internal friction angle (φ). Meanwhile, the growth of new crystals may locally disrupt pre-existing, weaker interparticle connections, leading to a decrease in cohesion (c). As the cementation solution concentration increases (above 1.00 mol/L), more crystals continue to grow. When the crystals on adjacent particle surfaces grow large enough for their "rough protrusions" to enter each other's effective interaction range, these

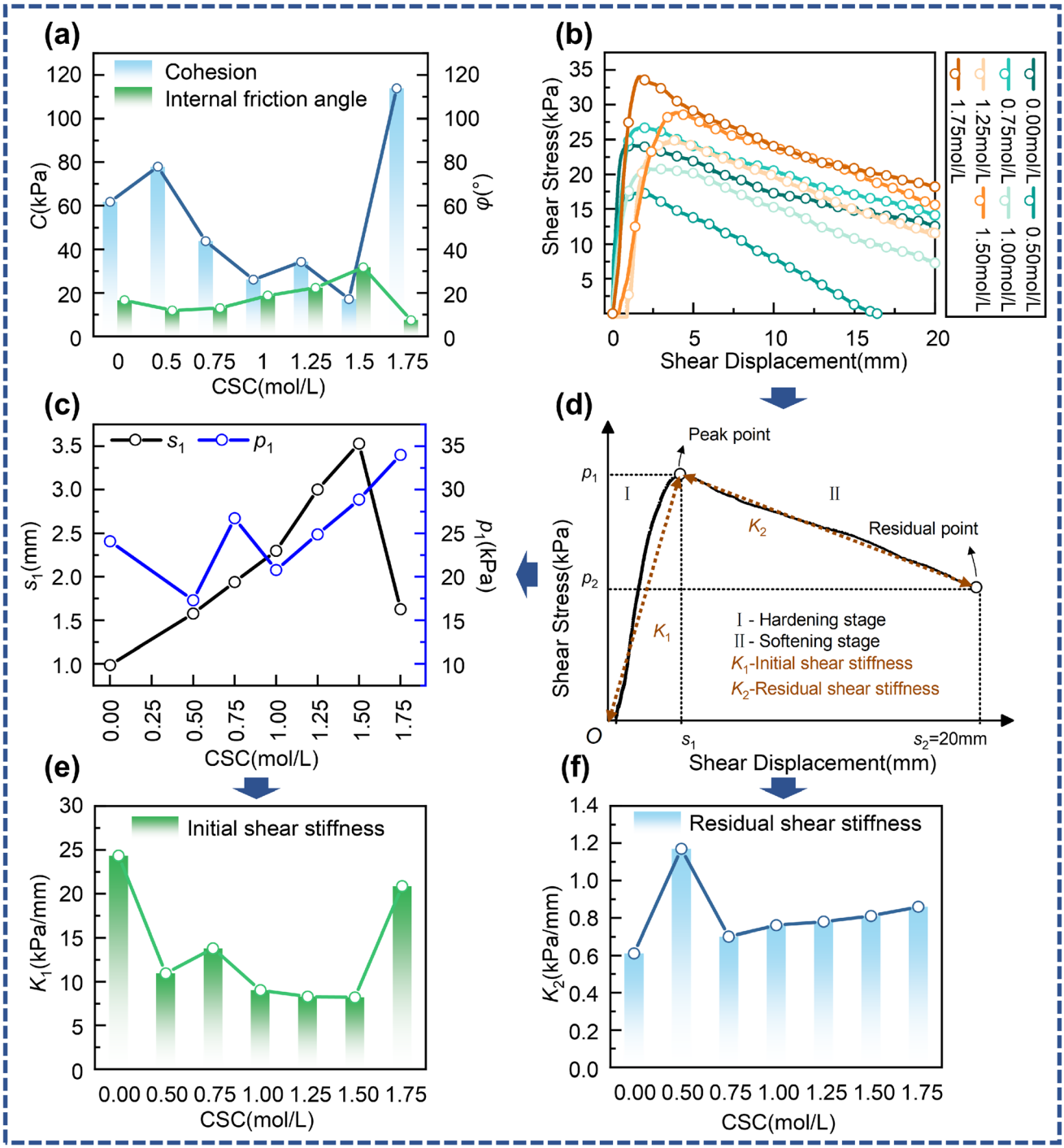

Fig. 4 **a** evolution of cohesion and internal friction angle of SICP-stabilized soil with cementation solution concentration, *CSC* represents cementation solution concentration; **b** the bond-slip curves of the SICP-stabilized anchorage interface; **c** peak shear strength and corresponding displacement of the anchorage interface in SICP-stabilized anchors at different cementation solution concentrations, P_1 represents peak shear strength, S_1 represents corresponding displacement of the peak shear strength; **d** schematic of typical characteristic points identified in pullout response; **e** initial shear stiffness of the anchorage interface in SICP-stabilized anchors at different cementation solution concentrations; **f** residual shear stiffness of the anchorage interface in SICP-stabilized anchors at different cementation solution concentrations

crystals may connect through further crystallization or physical interlocking. This achieves a transition from "particle surface modification" to "interparticle connection" (i.e., "chemical bridging"). This stable connection significantly enhances cohesion (c). However, once firm bridging forms, the relative sliding between particles

depends more on the shear failure of the bridges rather than on the friction of the original particle surfaces. This may cause the rate of increase in the internal friction angle (φ) to slow down or even decline.

4.2 Bond-slip behavior at the anchorage interface of the SICP-stabilized anchors

4.2.1 Mechanical parameters of the anchorage interface

Interface shear property tests were carried out on element specimens of SICP-stabilized anchors under different cementation solution concentrations. The resulting bond-slip curves (shear stress–displacement curves) are shown in Fig. 4b.

As shown in Fig. 4b, the bond-slip response of the SICP-stabilized anchorage interface exhibits strain-softening under all cementation solution concentrations. Compared to the unstabilized anchor (0.00 mol/L), the anchorage performance of the SICP-stabilized anchors is generally improved. To analyze the mechanical properties of the anchorage interface, the ultimate shear stress on the bond-slip curve is defined as the peak shear strength (as P_1) of the anchorage interface. The shear strength corresponding to a shear displacement of 20 mm is defined as the residual shear strength (as P_2). The slope before the peak is defined as the initial shear stiffness (as K_1), and the slope after the peak is defined as the residual shear stiffness (as K_2) (as shown in Fig. 4d). The relationships between these parameters (peak shear strength, initial shear stiffness, and residual shear stiffness) and the cementation solution concentration are depicted in Fig. 4c, e and Fig. 4f. More relevant information can be obtained from Table 4.

4.2.2 Effect of the cementation solution concentration

(1) Peak shear strength of the anchorage interface:

As shown in Fig. 4c, the peak shear strength of the anchorage interface of SICP-stabilized anchors and the corresponding displacement vary with the cementation solution concentration. The peak shear strength fluctuates with increasing cementation solution concentration below 1.00 mol/L. A linear growth trend is observed when the concentration exceeds 1.00 mol/L. The displacement corresponding to the peak shear strength indicates the shear deformation required to mobilize the interface's ultimate strength. This displacement increases roughly linearly with the cementation solution concentration, peaking at 1.50 mol/L, then declines sharply, highlighting the influence of cementation solution concentration on the initial shear stiffness of the anchorage interface.

(2) Initial shear stiffness of the anchorage interface:

Table 4 Mechanical parameters of pullout tests under different cementation solution concentrations (CSC)

CSC (mol/L)	P_1 (kPa)	S_1 (mm)	P_2 (kPa)	K_1 (kPa/mm)	K_2 (kPa/mm)
0.00	24.09	0.99	12.56	24.33	0.61
0.50	17.29	1.58	0.00	10.94	1.17
0.75	26.75	1.94	14.12	13.79	0.70
1.00	20.78	2.30	7.26	9.03	0.76
1.25	24.88	3.00	11.57	8.29	0.78
1.50	28.86	3.53	15.59	8.18	0.81
1.75	34.00	1.63	18.20	20.86	0.86

Figure 4e shows how the initial shear stiffness of the anchorage interface of SICP-stabilized anchors varies with cementation solution concentration. Compared to the unstabilized anchor (0.00 mol/L), the initial shear stiffness of the anchorage interface for SICP-stabilized anchors decreases within cementation solution concentrations below 1.5 mol/L, with minimal overall change. However, when the cementation solution concentration increases to 1.75 mol/L, the initial shear stiffness grows significantly, approaching that of the unstabilized anchor. This indicates that while SICP reinforcement has a degrading effect on the initial shear stiffness of the anchorage interface.

(3) Residual shear stiffness of the anchorage interface:

Figure 4f shows that compared to the unstabilized anchor (0.00 mol/L), SICP reinforcement has minimal effect on the residual shear stiffness of the anchorage interface. At a cementation solution concentration of 0.5 mol/L, the residual shear stiffness nearly doubles that of the unstabilized anchor. At other concentrations, it only increases slightly (under 20%). Thus, the residual shear stiffness is relatively insensitive to cementation solution concentration, showing almost no change between 0.75 and 1.75 mol/L.

4.3 Microstructural characteristics of shear band soil at the anchorage interface

4.3.1 SEM microstructure

Figure 5a presents the microstructural characteristics of shear band soil near the anchorage interface of SICP-stabilized anchors under different cementation solution concentrations, as obtained through SEM analysis. Comparative analysis reveals the following observations:

(1) With increasing cementation solution concentration, heterogeneous nucleation sites on soil particle surfaces progressively multiply. Crystal growth from these nucleation points gradually bridges flaky soil particles, transforming the soil's flocculent structure into a honeycomb-flocculent hybrid structure.

(2) As the concentration increases from 0.00 to 1.00 mol/L, a marked reduction in soil porosity occurs, with macropores being filled and converted to micropores. However, when the concentration exceeds 1.00 mol/L, further increases lead to renewed pore development (Fig. 5a).
(3) Cementation solution concentration significantly influences calcium carbonate crystal phase transitions. Below 1.00 mol/L, cuboidal calcite crystals become increasingly predominant, whereas above this threshold, acicular aragonite and spherical vaterite phases emerge with rising concentration.

The observed microstructural alterations are fundamentally caused by the fact that a fixed quantity of urease can only catalyze a limited urea hydrolysis reaction, establishing specific ammonia-carbon equilibria, while the 1:1 mass ratio of calcium chloride to urea in the cementation solution fails to align with the mass ratios dictated by these equilibria. Increasing the cementation solution concentration consequently elevates carbonate ion concentration without providing a sufficient calcium source. This triggers dissolution-reprecipitation phase transitions of calcium carbonate crystals under varying carbonate concentrations, which ultimately inhibits the complete transformation of amorphous calcium carbonate into pore-filling and particle-binding calcite crystals, thereby inducing the characteristic biphasic pore evolution pattern featuring an initial decrease followed by a subsequent increase in porosity.

To further quantify the pore structure characteristics of SICP-stabilized soil in the shear band, PCAS software was employed to perform quantitative pore characterization based on SEM microstructural images. The quantified parameters include porosity, probability entropy, and fractal dimension of pore size distribution. Porosity follows the conventional definition in soil mechanics. Due to the high randomness of pore orientation distribution in soils, probability entropy is adopted to characterize directional variations. The fractal dimension of pore size distribution reflects the inhomogeneity and complexity of pore size distributions, where higher fractal dimensions indicate more complex pore structures and greater size distribution inhomogeneity.

The specific steps of quantitative pore characterization involve: (1) grayscale segmentation of SEM images to obtain binarized images, (2) division of pore regions for geometric feature extraction, and (3) calculation of porosity, probability entropy, and fractal dimension of pore size distribution.

Table 5 presents the quantitative pore characterization parameters of SICP-stabilized soil in the shear band.

(1) As the cementation solution concentration increases, the porosity of the shear band SICP-stabilized soil first decreases and then increases (Fig. 5b). This further confirms that a fixed amount of urease catalyzes the hydrolysis of a fixed amount of urea, corresponding to a fixed quantity of calcium carbonate crystals that fill and bond the pores.
(2) Under different cementation solution concentrations, the probability entropy of the pore structure in the shear band SICP-stabilized soil exceeds 0.96, indicating that the cementation solution concentration has no significant effect on the directional variations of the pores.
(3) With increasing cementation solution concentration, the fractal dimension of pore porosity distribution initially increases and then decreases. When the concentration reaches the range of 0.75–1.50 mol/L, the fractal dimension increases significantly and stabilizes around 1.9. However, when the concentration further increases to 1.75 mol/L, the fractal dimension drops sharply to levels comparable to those at lower cementation solution concentrations. These findings further verify that once the cementation solution concentration reaches a certain threshold, the larger pores in the shear band SICP-stabilized soil are progressively filled to varying degrees by calcium carbonate crystals (e.g., calcite), forming small and micropores with diverse morphologies, which markedly increases pore distribution inhomogeneity. Upon further increasing the cementation solution concentration, phase transitions of calcium carbonate crystals occur, gradually releasing pores, reducing pore categories, and leading to a more homogeneous pore distribution.

4.3.2 XRD mineralogical composition

The XRD test result of shear band SICP-stabilized soil under different cementation solution concentrations is shown in Fig. 5c. It reveals that the main chemical components of SICP-stabilized soil remain dominated by silica from clay minerals. With the progression of mineralization, calcium carbonate crystals gradually appear, along with residual heavy metal components from the stabilized soil samples. Further analysis of the influence of cementation solution concentration on the mineralization composition of SICP-stabilized soil shows:

(1) At low concentrations (0.50–0.75 mol/L), urea hydrolysis proceeds slowly, with calcium carbonate crystals in the nucleation phase and not yet fully grown. Unreacted urea is present, exhibiting broad

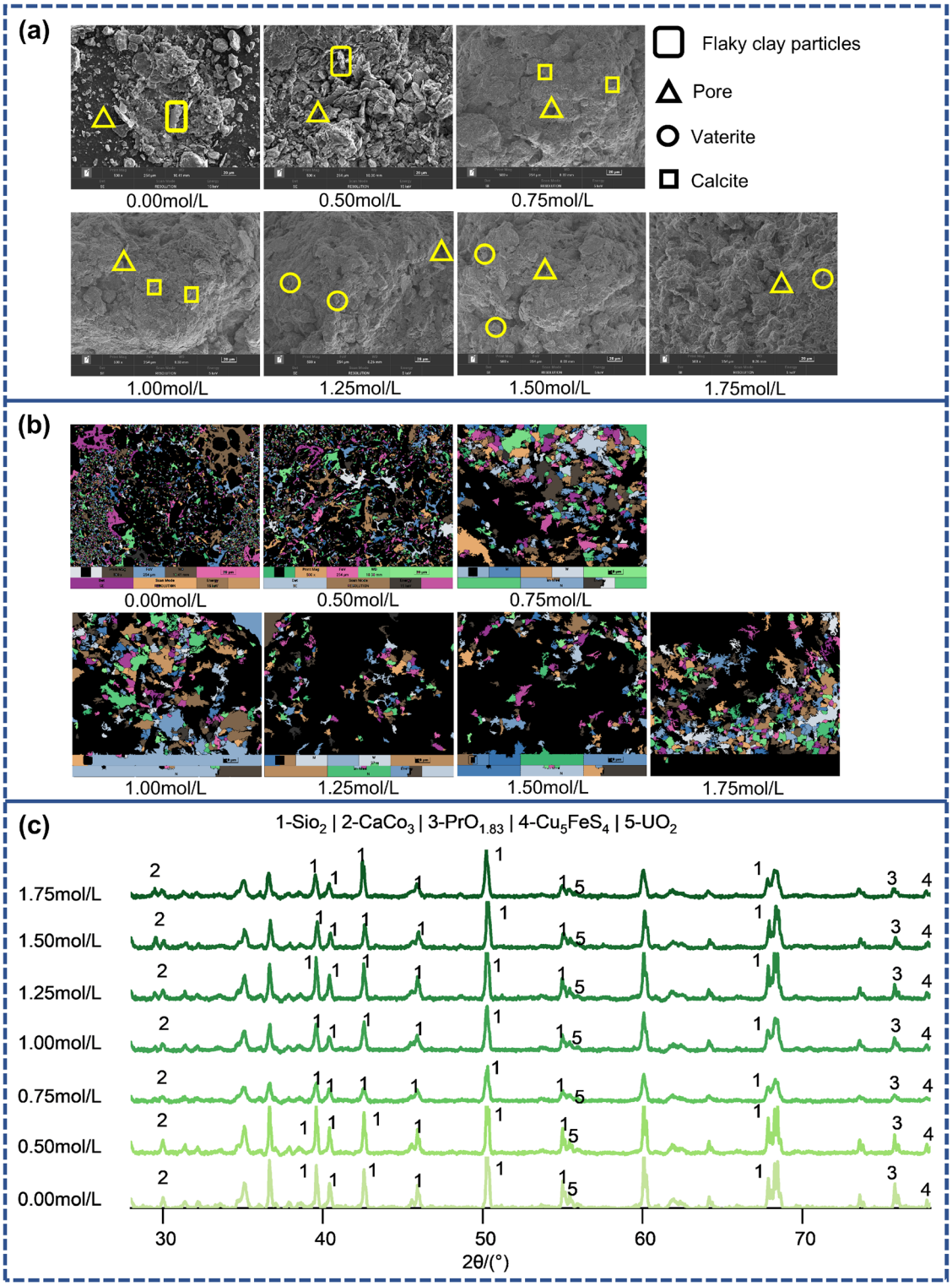

Fig. 5 **a** microstructure of shear band SICP-stabilized soil at different cementation solution concentrations; **b** pore identification in SEM images; **c** mineralization composition analysis of shear band SICP-stabilized soil

and low-intensity calcium carbonate peaks along with low calcium carbonate content.

(2) At medium concentration (1.00 mol/L), the proportions of urease, urea, and calcium source are well-matched, resulting in more complete urea hydrolysis. Calcium carbonate precipitates as highly crystalline calcite, exhibiting sharp peaks with maximum intensity and the highest calcium carbonate content.

(3) At high concentrations (1.25–1.75 mol/L), the calcium source is insufficient to react with all carbonate ions from urea hydrolysis. In this high-carbonate environment, calcium carbonate precipitates rapidly but with low crystallinity, primarily forming amorphous or metastable vaterite that cannot further develop into highly crystalline calcite. This phenomenon is exhibited as calcium carbonate peaks of moderate intensity (possibly broadened) with intermediate calcium carbonate content.

4.4 Relationship between macro- and micro-scale parameters

4.4.1 Relationship between microstructural parameters and direct shear strength parameters

Figure 6c, f illustrates the variations of cohesion (c) of the SICP-stabilized soil with porosity and the fractal dimension of pore size distribution. As porosity and the fractal dimension increase, cohesion (c) initially rises and then declines, reaching its maximum at a concentration of 1.75 mol/L. This trend may be attributed to the following mechanisms: at lower concentrations ($\leq$ 0.5 mol/L), the soil cohesion primarily relies on the bonding of natural clay particles, showing little difference from the unstabilized soil. As the cementation solution concentration increases (0.75–1.50 mol/L), the hydrolysis of urea and the calcium source become relatively well-matched, leading to the formation of stable calcite. The effective filling of pores by these crystals creates micropores, resulting in a significant increase in pore structure complexity. During this stage, crystal growth may favor "physical roughening", which disrupts pre-existing interparticle bonds, shifting the primary contribution to strength toward an increase in the internal friction angle. When the concentration further increases to 1.75 mol/L, the relatively high concentration of carbonate ions and the insufficient calcium source deteriorate the crystallization environment for calcium carbonate. This promotes the formation of metastable aragonite or vaterite, which cannot pack densely or fill pores as effectively as calcite, leading to a gradual release of pores, an increase in porosity, and a more homogeneous pore distribution. Meanwhile, "chemical bridging" becomes dominant. The massive amount of generated microcrystals interweave, providing strong physicochemical adsorption forces that significantly enhance interparticle cohesion. The expressions for the fitting curves C and F, along with the related parameters, are listed in Table 6.

4.4.2 Relationship between microstructural parameters and interface shear strength parameters

Figure 6a, d illustrates the variations of the interface peak shear strength (P_1) of the SICP-stabilized element specimens with porosity and the fractal dimension of pore size distribution. It is important to note that the data for the 0.5 mol/L cementation solution concentration were excluded from this analysis (The 0.5 mol/L data are questioned due to its poor fit and fundamentally different residual shear strength in Fig. 4b). As porosity and the fractal dimension increase, the interface peak shear strength P_1 generally exhibits a trend of first increasing and then decreasing, reaching its maximum at a concentration of 1.75 mol/L. This behavior can be explained by the following mechanisms: When the cementation solution concentration is at a relatively low level (0.75–1.50 mol/L), the growth of calcite crystals reduces porosity while simultaneously creating a complex pore structure. During this stage, the soil becomes stiffer and frictional resistance is enhanced. The soil near the shear band primarily relies on the internal friction angle to resist shear (leaning toward "physical roughening", though the contribution of "chemical bridging" increases). However, the cementation at the interface is non-uniform and discontinuous, resulting in limited peak shear strength. When the concentration increases to 1.75 mol/L, a phase transformation of the crystals to aragonite/vaterite occurs, leading to a moderate

Table 5 Quantitative pore characterization parameters of shear band SICP-stabilized soil

CSC(mol/L)	0.00	0.50	0.75	1.00	1.25	1.50	1.75
Porosity	38.78	38.39	51.50	47.52	24.23	27.77	33.76
Probability entropy	0.992	0.993	0.974	0.978	0.968	0.972	0.989
Fractal dimension of pore size distribution	1.2113	1.2099	1.8784	1.9843	1.8473	1.9744	1.4442

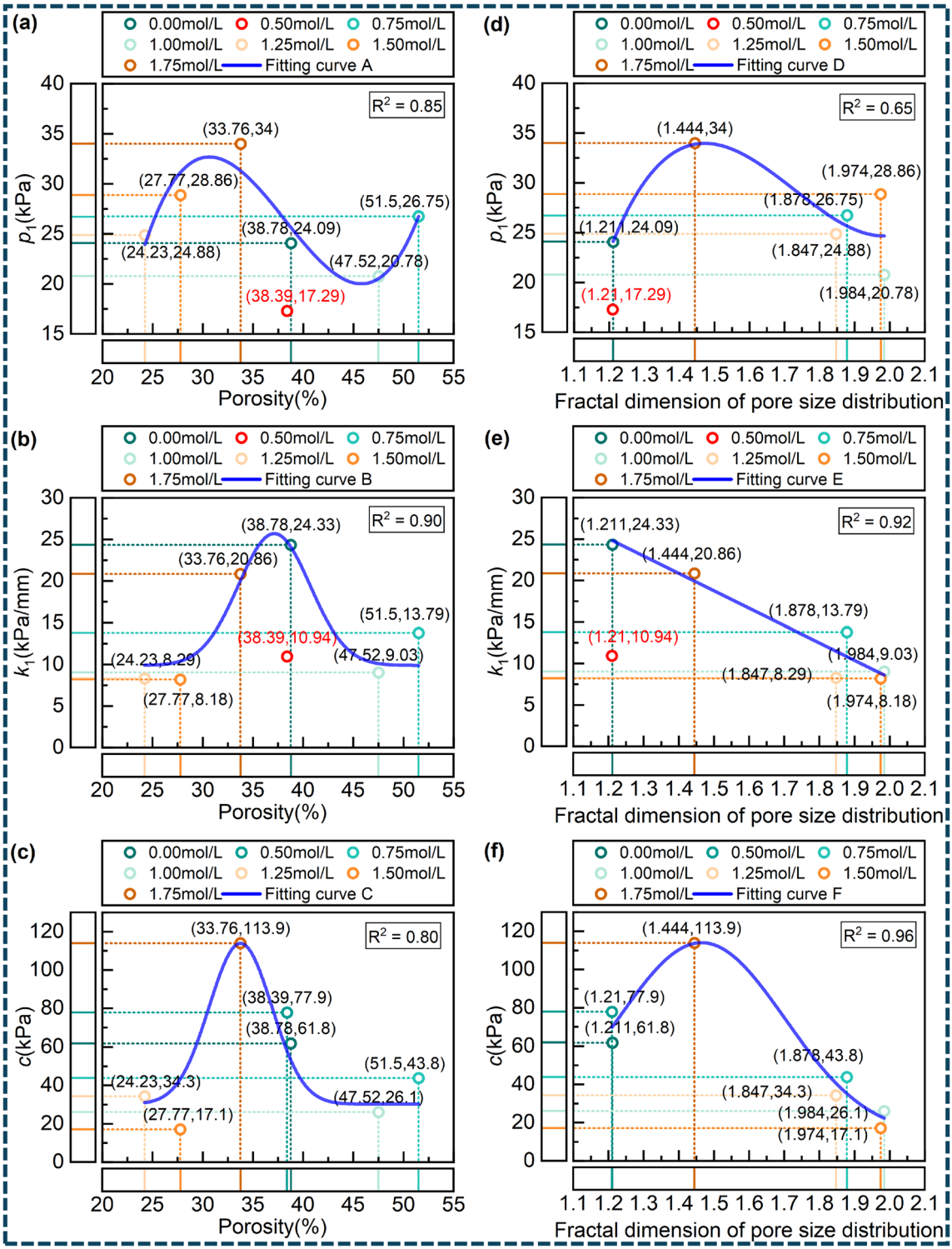

Fig. 6 **a** Relationship between peak shear strength (P_1) and porosity; **b** relationship between initial shear stiffness (K_1) and porosity; **c** relationship between cohesion (c) and porosity; **d** relationship between peak shear strength (P_1) and fractal dimension of pore size distribution; **e** relationship between initial shear stiffness (K_1) and fractal dimension of pore size distribution; **f** relationship between cohesion (c) and fractal dimension of pore size distribution

recovery in porosity and the formation of a simpler, more homogeneous cementation-pore composite structure. At this stage, a continuous, uniform, and tough cementation transition layer forms around the interface (dominated by

the "chemical bridging" effect), thereby significantly enhancing the peak strength. The expressions for the fitting curves A and D, along with the related parameters, are listed in Table 6.

Figure 6b, e illustrates the variations of the interface initial shear stiffness (K_1) of the SICP-stabilized element specimens with porosity and the fractal dimension of pore size distribution. A key characteristic is revealed by comparing these two relationships: High K_1 values consistently occur in samples on the side of lower pore fractal dimension, regardless of their porosity level. This phenomenon may be explained as follows: When the cementation solution concentration is at a relatively low level (0.75–1.50 mol/L), the growth of calcite crystals is uneven. The "physical roughening" effect forms a complex pore network (high pore fractal dimension), resulting in an uneven distribution of cementitious material at the interface, which contains weak points or stress concentration points. During the initial loading phase, these weak points undergo micro-yielding or adjustment first, leading to an overall decrease in initial stiffness. When the concentration increases to 1.75 mol/L, aragonite/vaterite microcrystals uniformly coat the soil particles in the shear band, forming a continuous and dense cementation layer (low pore fractal dimension). The "chemical bridging" effect provides rigid chemical connections, resulting in a high K_1. The expressions for the fitting curves B and E, along with the related parameters, are listed in Table 6.

5 Conclusions

This study conducted systematic experimental investigations on the mechanical properties of SICP-stabilized soil and the mechanical characteristics of the anchorage interface under different cementation solution concentrations. Microstructural analysis was performed on the shear band of the stabilized soil at the anchorage interface. The obtained findings can be summarized as follows:

(1) The urease extracted from soybean powder exhibits maximum specific activity at a concentration of 40 g/L; therefore, 40 g/L soybean powder concentration is recommended as the optimal urease source.
(2) The SICP-stabilized soil demonstrates strain-hardening behavior under shear loading. The cohesion and internal friction angle of the stabilized soil show a "see-saw" complementary relationship with increasing cementation solution concentration.
(3) The bond-slip response at the anchorage interface displays strain-softening behavior. When the cementation solution concentration exceeds 1.00 mol/L, the ultimate shear strength of the interface (P_1) exhibits a distinct linear growth trend with increasing concentration. However, the residual shear stiffness (K_2) shows relatively low sensitivity to variations in cementation solution concentration.
(4) Cementation solution concentration governs pore structure evolution and anchorage performance by regulating calcium carbonate crystal growth. Lower concentrations favor "physical roughening", enhancing friction (φ) but limiting P_1 and K_1. Higher concentrations promote "chemical bridging," which simultaneously enhances cohesion (c), P_1 and K_1.

These findings provide a fundamental mechanistic understanding for the potential field application of SICP in ground anchor enhancement. The optimal cementation solution concentration range identified (1.00–1.75 mol/L) provides a reference for designing cost-effective SICP treatments in practical anchor reinforcement. However, direct field application must consider key limitations of this study, including the differences between laboratory-mixed, uniformly stabilized specimens and in situ injection methods, as well as the controlled laboratory conditions versus variable field environments.

Table 6 Summary of fitting curves for macro–micro relationships

Fitting curve	Equation	Parameters				R^2
		a	b	c	d	
A	$y = a + bx + cx^2 + dx^3$	− 332.145	30.650	− 0.835	0.007	0.85
B	$y = a + be^{-\frac{(x-c)^2}{2d^2}}$	9.875	15.832	37.121	3.576	0.90
C	$y = a + be^{-\frac{(x-c)^2}{2d^2}}$	30.200	83.699	33.760	3.118	0.80
D	$y = a + bx + cx^2 + dx^3$	− 647.727	1230.676	− 728.372	140.574	0.65
E	$y = a + bx$	50.200	− 20.959	–	–	0.92
F	$y = a + be^{-\frac{(x-c)^2}{2d^2}}$	13.206	100.860	1.465	0.237	0.96

These conclusions are derived from direct shear tests and interface shear tests. Their applicability for predicting the load-bearing capacity of engineering-scale SICP-stabilized anchors requires further validation through cross-scale experimental studies. In the future, our team will investigate the effects of urease type/content, cementation solution injection methods, and grouting properties on the interface behavior of SICP-stabilized anchors.

Acknowledgements This work was sponsored by National College Student Innovation and Entrepreneurship Training Program (Grant number: S202411527103), National Key R&D Program of China (Grant number: 2023YFC3009400), National Natural Science Foundation of China (Grant numbers: 52578400), and Natural Science Foundation of Hunan Province (Grant number: 2025JJ50294). The authors appreciate their supports.

Author contributions Genbao Zhang provided idea, equipments, and supervision. Xiao Luo conducted the tests and wrote the main manuscript. Mingdong Li and Changjie Xu provided funding, equipments, and supervision. Lanting Deng helped to write and edit the manuscript. Siqing Li, Yukang Liu, Zhining Wang, and Zhongbiao Li helped to conduct the tests. All authors reviewed the manuscript.

Data availability All of the data that support the findings of this study are available from the corresponding author upon request.

Declarations

Conflict of interest The authors declare no competing interests.

References

1. Ahenkorah I, Rahman MM, Karim MR, Beecham S (2024) Characteristics of MICP-and EICP-treated sands in simple shear conditions: a benchmarking with the critical state of untreated sand. Géotechnique 74(13):1649–1663. https://doi.org/10.1680/jgeot.22.00329
2. Alotaibi E, Arab MG, Abdallah M, Nassif N, Omar M (2022) Life cycle assessment of biocemented sands using enzyme induced carbonate precipitation (EICP) for soil stabilization applications. Sci Rep 12(1):6032. https://doi.org/10.1038/s41598-022-09723-7
3. Alwalan M, Almajed A, Lemboye K, Alnuaim A (2023) Direct shear characteristics of enzymatically cemented sands. KSCE J Civ Eng 27(4):1512–1525. https://doi.org/10.1007/s12205-023-0817-2
4. Chen C, Zhang G, Zornberg JG, Morsy AM, Zhu S, Zhao H (2018) Interface behavior of tensioned bars embedded in cement-soil mixtures. Constr Build Mater 186:840–853. https://doi.org/10.1016/j.conbuildmat.2018.07.211
5. Chen C, Zhang G, Zornberg JG, Morsy AM, Huang J (2020) Interface bond behavior of tensioned glass fiber-reinforced polymer (GFRP) tendons embedded in cemented soils. Constr Build Mater 263:120132. https://doi.org/10.1016/j.conbuildmat.2020.120132
6. Chen C, Zhu S (2024) Element-scale pullout test study on the mechanical behavior of grouted anchor–soil interface subjected to ground pressure. Acta Geotech 19(8):5433–5447. https://doi.org/10.1007/s11440-024-02256-5
7. Chen Y, Gao Y, Ng CW, Guo H (2021) Bio-improved hydraulic properties of sand treated by soybean urease induced carbonate precipitation and its application Part 1: water retention ability. Transp Geotech 27:100489. https://doi.org/10.1016/j.trgeo.2020.100489
8. Cui M, Lai H, Wu S, Chu J (2024) Comparison of soil improvement methods using crude soybean enzyme, bacterial enzyme or bacteria-induced carbonate precipitation. Géotechnique 74(1):18–26. https://doi.org/10.1680/jgeot.21.00131
9. Dong X, Fang L, Ma Y, Hu Q, Li R (2024) Experimental study on the strength of loess solidified by soybean urease-induced calcium carbonate precipitation. China Earthq Eng J 46(05):1009–1020. https://doi.org/10.20000/j.1000-0844.20231125002
10. Du Y, Li H, Chicas SD, Huo L (2022) Progress and perspectives of geotechnical anchor bolts on slope engineering in China. Front Environ Sci 10:928064. https://doi.org/10.3389/fenvs.2022.928064
11. Gao Y, Meng H, He J, Qi Y, Hang L (2020) Field trial on use of soybean crude extract for carbonate precipitation and wind erosion control of sandy soil. J Cent South Univ 27(11):3320–3333. https://doi.org/10.1007/s11771-020-4549-x
12. Gao Y, Hua C, Li Y, He J, Dai Z, Shen Y (2022) Biological solutions for the remediation of cracks in ancient earthen structures: experimental studies. J Mater Civ Eng 34(11):04022312. https://doi.org/10.1061/(ASCE)MT.1943-5533.0004453
13. Gao Y, Hua C, Ke T (2022) Field test on soybean-urease induced calcite precipitation (SICP) for desert sand stabilization against the wind-induced erosion. Sustainability 14(22):15474. https://doi.org/10.3390/su142215474
14. He J, Huang A, Ji J, Qu S, Hang L (2023) Enzyme induced carbonate precipitation with fibers for the improvement of clay soil slopes against rainfall and surface runoff erosions. Transp Geotech 42:101074. https://doi.org/10.1016/j.trgeo.2023.101074
15. He J, Liu Y, Liu L, Yan B, Li L, Meng H, Hang L, Qi Y, Gao Y (2023) Recent development on optimization of bio-cementation for soil stabilization and wind erosion control. Biogeotechnics 1(2):100022. https://doi.org/10.1016/j.bgtech.2023.100022
16. Li M, Liu W, Zhang J, Lang C, Xu G, Zhu L, Tang Q (2025) Soybean-urease-induced $CaCO_3$ precipitation as a new geotechnique for improving expansive soil. Acta Geotech 20(4):1877–1890. https://doi.org/10.1007/s11440-024-02481-y
17. Li Y, Li Y, Guo Z, Xu Q (2023) Durability of MICP-reinforced calcareous sand in marine environments: laboratory and field experimental study. Biogeotechnics 1(2):100018. https://doi.org/10.1016/j.bgtech.2023.100018
18. Liu K, Jiang N, Qin J, Wang Y, Tang C, Han X (2021) An experimental study of mitigating coastal sand dune erosion by microbial-and enzymatic-induced carbonate precipitation. Acta Geotech 16(2):467–480. https://doi.org/10.1007/s11440-020-01046-z
19. Liu Y, Gao Y, He J, Zhou Y, Geng W (2023) An experimental investigation of wind erosion resistance of desert sand cemented by soybean-urease induced carbonate precipitation. Geoderma 429:116231. https://doi.org/10.1016/j.geoderma.2022.116231
20. Pan X, Jia J (2025) Time-dependent system reliability analysis of anchor-reinforced slopes based on surrogate models. Comput Geotech 184:107257. https://doi.org/10.1016/j.compgeo.2025.107257

21. Sun S, Jia X, Xiao J (2022) Research status and development trend analysis of geotechnical pre-stressed anchoring technology. Saf Coal Mines 53(3):213–220. https://doi.org/10.13347/j.cnki.mkaq.2022.03.032
22. Whiffin VS, Van Paassen LA, Harkes MP (2007) Microbial carbonate precipitation as a soil improvement technique. Geomicrobiol J 24(5):417–423. https://doi.org/10.1080/01490450701436505
23. Wang R, Wang G, Zhang L, Sun F, Li B (2025) Macro-micro damage and energy release rates of fractured sandstone subjected to dry-wet cycles. J Rock Mech Geotech Eng 17(6):3563–3576. https://doi.org/10.1016/j.jrmge.2024.09.055
24. Wang W, Wu S, Chu J, Tun K (2025) Biocementation for beach erosion control using seawater extracted soybean enzyme. Acta Geotech. https://doi.org/10.1007/s11440-025-02654-3
25. Wang Y, Chen W, Li P, Yin Z, Yin J, Jiang N (2024) Soil improvement using biostimulated MICP: mechanical and biochemical experiments, reactive transport modelling, and parametric analysis. Comput Geotech 172:106446. https://doi.org/10.1016/j.compgeo.2024.106446
26. Wang Y, Wang Z, Chen Y, Cao T, Yu X, Rui P (2023) Experimental study on bio-treatment effect of the dredged Yellow River silt based on soybean urease induced calcium carbonate precipitation. J Build Eng 75:106943. https://doi.org/10.1016/j.jobe.2023.106943
27. Wang Y, Chen H, Song Y, Wang Z, Zhong Y, Zhang B (2024) Experimental study on water stability of Yellow River silt solidified by soybean-urease induced carbonate precipitation. J Hydraul Eng 55(01):71–79. https://doi.org/10.13243/j.cnki.slxb.20230344
28. Wang Y, Chen Y, Marchelina N (2025) Crack repairing performance by soybean urease induced calcium carbonate precipitation (SICP) combined with fibers and lightweight aggregates. Constr Build Mater 458:139678. https://doi.org/10.1016/j.conbuildmat.2024.139678
29. Xu K, Huang M, Liu Z, Cui M, Li S (2023) Mechanical properties and disintegration behavior of EICP-reinforced sea sand subjected to drying-wetting cycles. Biogeotechnics 1(2):100019. https://doi.org/10.1016/j.bgtech.2023.100019
30. Yang Y, Liu Z, Yang Q, Guo C, Hu Y, Xiao H, Xia D, Wu J, Lu Y, Hu X, Xia Z, Zhou M, Xu W, Chen J, Liu D (2025) Synergistic application of sandy ecological substrate through high-calcium fly ash and enzyme-induced carbonate precipitation integration. J Environ Chem Eng. https://doi.org/10.1016/j.jece.2025.116783
31. Yuan H, Shi Q, Li J, Zhao Z (2023) Effect of freeze–thaw cycling on mechanical properties of Na-montmorillonite modified EICP-treated silty sand. Case Stud Constr Mater 19:e02641. https://doi.org/10.1016/j.cscm.2023.e02641
32. Zhang G, Chen C, Zornberg JG, Morsy AM, Mao F (2020) Interface creep behavior of grouted anchors in clayey soils: effect of soil moisture condition. Acta Geotech 15(8):2159–2177. https://doi.org/10.1007/s11440-019-00907-6
33. Zhang G, Chen C, Sun J, Li K, Xiao F, Wang Y, Chen M, Huang J, Wang X (2022) Mixture optimisation for cement-soil mixtures with embedded GFRP tendons. J Mater Res Technol 18:611–628. https://doi.org/10.1016/j.jmrt.2022.02.076
34. Zhang G, Xu C, Wang Y, Sun J, Ding H, Zhu S, Zou Z, Azzani HA, Li Z, Li D, Wang X (2024) Experimental and data-driven prediction for the impact of free/bond lengths of element specimen on interface characterization of ground anchors. Ocean Eng 309:118468. https://doi.org/10.1016/j.oceaneng.2024.118468
35. Zhang G, Xu C, Wang D, Wang Y, Sun J, Zhu S, Morsy AM, Liu Z, Wang X (2024) Machine learning-based modeling of interface creep behavior of grouted soil anchors with varying soil moistures. Transp Geotech 48:101299. https://doi.org/10.1016/j.trgeo.2024.101299
36. Zhang K, Tang C, Jiang N, Pan X, Liu B, Wang Y, Shi B (2023) Microbial-induced carbonate precipitation (MICP) technology: a review on the fundamentals and engineering applications. Environ Earth Sci 82(9):229. https://doi.org/10.1007/s12665-023-10899-y
37. Zhang X, Wang H, Wang Y, Wang J, Cao J, Zhang G (2025) Improved methods, properties, applications and prospects of microbial induced carbonate precipitation (MICP) treated soil: a review. Biogeotechnics 3(1):100123. https://doi.org/10.1016/j.bgtech.2024.100123
38. Zhang Y, Zhou Y, Geng W, Yan B, Hang L, He J, Gao Y (2025) The influence of SICP treatment composition on the performance of liquefaction resistance of soils. Soil Dyn Earthq Eng 195:109397. https://doi.org/10.1016/j.soildyn.2025.109397
39. Zhao W, Han J, Chen Y, Jia P, Li S, Li Y, Zhao Z (2018) A numerical study on the influence of anchorage failure for a deep excavation retained by anchored pile walls. Adv Mech Eng 10(2):1687814018756775. https://doi.org/10.1177/1687814018756775
40. Zhou Y, Zhang Y, Geng W, He J, Gao Y (2023) Evaluation of liquefaction resistance for single-and multi-phase SICP-treated sandy soil using shaking table test. Acta Geotech 18(11):6007–6025. https://doi.org/10.1007/s11440-023-02008-x
41. Zhu S, Chen C, Zhang G, Du C (2022) Theoretical and experimental investigations of anchoring force loss behavior for pre-stressed ground anchors. Can Geotech J 59(9):1587–1601. https://doi.org/10.1139/cgj-2021-0220
42. Zhu S, Chen C, Du C (2023) Interface stress relaxation behavior of grouted anchors in red clay: experimental study and a disturbed state concept-based theoretical model. Acta Geotech 18(6):3287–3306. https://doi.org/10.1007/s11440-022-01693-4

Authors and Affiliations

Genbao Zhang[1,2] · Xiao Luo[3] · Siqing Li[1] · Lanting Deng[3] · Yukang Liu[1] · Zhining Wang[1] · Zhongbiao Li[1] · Mingdong Li[4] · Changjie Xu[2]

✉ Genbao Zhang
genbao@hncu.edu.cn

Xiao Luo
luoxiao@hncu.edu.cn

Siqing Li
1731930656@qq.com

Lanting Deng
1312281570@qq.com

Yukang Liu
2437897034@qq.com

Zhining Wang
2070139983@qq.com

Zhongbiao Li
2519078830@qq.com

Mingdong Li
ytlimd@163.com

Changjie Xu
xucj@zju.edu.cn

[1] College of Civil Engineering, Hunan City University, Yiyang 413000, Hunan, China

[2] School of Civil Engineering and Architecture, East China Jiaotong University, Nanchang 330013, Jiangxi, China

[3] School of Civil Engineering, Xiangtan University, Xiangtan 411105, Hunan, China

[4] School of Civil and Architectural Engineering, East China University of Technology, Nanchang 330013, Jiangxi, China